

# A Multispecies Exclusion Process with Fusion and Fission of Rods: a model inspired by Intraflagellar Transport

Swayamshree Patra and Debashish Chowdhury

Department of Physics, Indian Institute of Technology Kanpur, 208016, India

**Abstract:** We introduce a multispecies exclusion model where length-conserving probabilistic fusion and fission of the hard rods are allowed. Although all rods enter the system with the same initial length  $\ell = 1$ , their length can keep changing, because of fusion and fission, as they move in a step-by-step manner towards the exit. Two neighboring hard rods of lengths  $\ell_1$  and  $\ell_2$  can fuse into a single rod of longer length  $\ell = \ell_1 + \ell_2$  provided  $\ell \leq N$ . Similarly, length-conserving fission of a rod of length  $\ell' \leq N$  results in two shorter daughter rods. Based on the extremum current hypothesis, we plot the phase diagram of the model under open boundary conditions utilizing the results derived for the same model under periodic boundary condition using mean-field approximation. The density profile and the flux profile of rods are in excellent agreement with computer simulations. Although the fusion and fission of the rods are motivated by similar phenomena observed in Intraflagellar Transport (IFT) in eukaryotic flagella, this exclusion model is too simple to account for the quantitative experimental data for any specific organism. Nevertheless, the concepts of ‘flux profile’ and ‘transition zone’ that emerge from the interplay of fusion and fission in this model are likely to have important implications for IFT and for other similar transport phenomena in long cell protrusions.

Non-equilibrium stationary state (NESS) of a driven system [1–3] is the counterpart of the state of equilibrium in a thermodynamic system. Totally asymmetric simple exclusion process (TASEP) [4–6] is a paradigmatic model for theoretical studies of the fundamental physical principles underlying NESS in systems of interacting self-driven particles.

A non-vanishing average uni-directional flow of particles through the system in its stationary state is a *macroscopic* indicator of the fact that steady state of TASEP is never in equilibrium. Under open boundary conditions (OBC), the density profile, which depicts the average stationary site occupational probabilities, is another *macroscopic* characteristic of the NESS of TASEP. Both these fundamental macroscopic characteristics of the NESS of TASEP can be computed, as averages, from the stationary configurational probabilities  $\{P^{ss}(C)\}$  and the corresponding probability currents  $\{J^{ss}(C \rightarrow C')\}$ , which together provide a *complete and unique microscopic* description of each NESS of TASEP [7].

In more general formulations of TASEP, the particles are replaced by hard rods, each of length  $\ell$ , where the length of the rods are measured in the units of lattice spacing [8–10]. From now onwards we will refer to particles also as rods with  $\ell = 1$ . Multi-species TASEP are known to exhibit richer varieties of phenomena compared to those in single-species TASEP [11]. Both single-species and multi-species TASEP, and their various extensions, have also found applications in modeling collective phenomena at many scales, starting from macroscopic vehicular traffic on highways to molecular motor traffic on filamentous tracks in living cells [12–20].

The distinct species of rods can be distinguished by either their length or their distinct kinetics (or both). In this letter we study an exclusion process with  $N$  ( $N > 1$ ) allowed species of rods,  $\ell$ -th species having length  $\ell$  (in the units of lattice spacing), where the species are *interconvertible* because of the ongoing *fusion* and *fission*

of the rods. Two rods of length  $\ell'$  and  $\ell''$  ( $\ell', \ell'' = 1, 2, 3, \dots, N$ ) in contact with each other are allowed to fuse resulting in a train of length  $\ell = \ell' + \ell''$ , provided  $\ell \leq N$ . Similarly, a rod of length  $\ell$  ( $\ell \leq N$ ) can split into two trains of lengths  $\ell'''$  and  $\ell''''$ .

The model developed in this letter is motivated by directed stochastic transport of membrane-bound cargoes in a *flagellum* (also called a cilium) which is a long protrusion found in some eukaryotic cells (for example, unicellular eukaryote *Chlamydomonas reinhardtii*). Because of their superficial similarities with cargo trains hauled along railway tracks, these cargoes are called Intra-flagellar transport (IFT) trains [21–24]. The IFT trains are distinct from train-like clusters reported earlier [25, 26]. Although the processes of fusion and fission of the rods in our model is motivated by IFT, this model is not intended to account for experimental data in any specific flagellated cell. Instead, the model focusses on the consequences of ongoing fusion and fission on the collective spatio-temporal organization of the  $N$  species of interconvertible particles in the NESS of the system.

By a combination of mean-field theory (MFT) and Monte Carlo (MC) simulations, we demonstrate qualitatively distinct features of the density profile and flux in this model. The density profile exhibits a “transition zone” (TZ) whose thickness depends on the fusion-fission kinetics. We introduce the concept of “flux profile” to highlight the relative contributions of the interconvertible species of particles and rods to the overall flux as they move forward along the lattice.

*Model* – The track is denoted by a one-dimensional lattice where each site is labelled by the integer index  $i$  ( $i = 1, \dots, L$ ); the sites  $i = 1$  and  $i = L$  correspond to the two boundaries at the entrance and the exit, respectively (see Fig.1). Only rods of length  $\ell = 1$  enter the 1-D lattice from the leftmost site ( $i = 1$ ) with rate  $\alpha$ . But the rods of all lengths  $\ell$  ( $\ell = 1, 2, \dots, N$ ) exit from right boundary ( $i = L$ ) with a length-independent rate  $\beta$ .



TABLE I. Summary of results under PBC for N=3

$\ell$ -dependent Quantities			Other Quantities		
Quantity	$\ell = 1$	$\ell = 2$	$\ell = 3$	Quantity	Expression
$\langle \mathcal{P}_\ell \rangle$	$\zeta_{3,1}$	$\zeta_{3,2} - \frac{2}{9}\zeta_{3,1}$	$\frac{\rho_c}{3} - \frac{5}{27}\zeta_{3,1} - \frac{2}{3}\zeta_{3,2}$	$\mathcal{J}_{mass}$	$\frac{27p\rho_c(1-\rho_c)}{16\zeta_{3,1}+9(3+2\zeta_{3,2}-2\rho_c)}$
$\langle \mathcal{J}_\ell \rangle$	$\frac{27p(1-\rho_c)\zeta_{3,1}}{16\zeta_{3,1}+9(3+2\zeta_{3,2}-2\rho_c)}$	$\frac{3p(1-\rho_c)(9\zeta_{3,2}-2\zeta_{3,1})}{16\zeta_{3,1}+9(3+2\zeta_{3,2}-2\rho_c)}$	$\frac{p(1-\rho_c)(9\rho_c-5\zeta_{3,1}-18\zeta_{3,2})}{16\zeta_{3,1}+9(3+2\zeta_{3,2}-2\rho_c)}$	$\langle \ell \rangle$	$\frac{27\rho_c}{(9\rho_c+16\zeta_{3,1}+9\zeta_{3,2})}$
$\langle \mathcal{F}_\ell \rangle$	$\frac{27\zeta_{3,1}}{9\rho_c+16\zeta_{3,1}+9\zeta_{3,2}}$	$\frac{27\zeta_{3,2}-6\zeta_{3,1}}{9\rho_c+16\zeta_{3,1}+9\zeta_{3,2}}$	$\frac{9\rho_c-5\zeta_{3,1}-18\zeta_{3,2}}{9\rho_c+16\zeta_{3,1}+9\zeta_{3,2}}$	$\sqrt{\langle \ell^2 \rangle}$	$\sqrt{\frac{81\rho_c-42\zeta_{3,1}-54\zeta_{3,2}}{(9\rho_c+16\zeta_{3,1}+9\zeta_{3,2})}}$

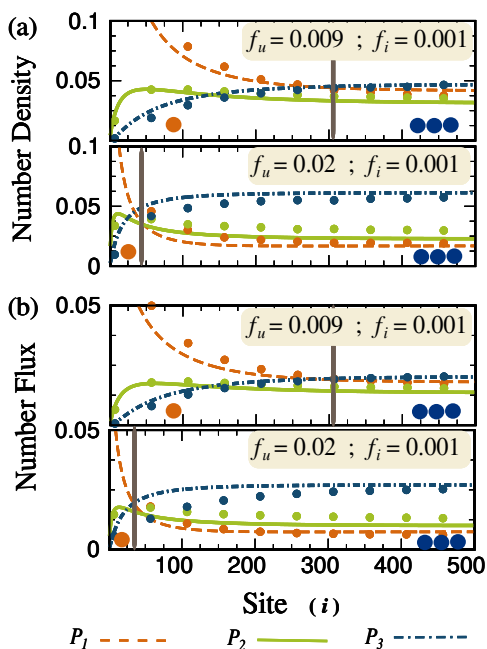


FIG. 3. (a) Number-Density Profile, and (b) Number-Flux Profile under OBC in the Transition Zone for  $N = 3$  and different combination of  $f_u$  and  $f_i$  mentioned in the figures.  $\alpha = 0.15$  and  $\beta = 0.85$  for all the cases (Lines-MFT ; Dots-Simulation).

appears at the coverage density  $\rho_c^* = \sqrt{\ell}/(\sqrt{\ell}+1)$ . Under PBC, in the limit  $K \rightarrow 0$ , rods longer than  $\ell = 1$  are practically non-existent in the NESS, irrespective of the initial conditions, and hence  $\rho_c^* \rightarrow 1/2$ . But in the opposite limit  $K \rightarrow \infty$ ,  $\rho_c^* \rightarrow \sqrt{2}/(\sqrt{2}+1)$  and  $\rho_c^* \rightarrow \sqrt{3}/(\sqrt{3}+1)$  for  $N=2$  and  $N=3$ , respectively. Thus, by tuning  $K$ , we can induce a transition from a regime where the track is populated almost exclusively by particles (i.e., rods of length  $\ell = 1$ ) to a regime where practically all the rods on the lattice have length  $\ell = N$ . Hence, over the range  $0.1 < K < 10$  regime, where  $f_u$  and  $f_i$  are comparable, a

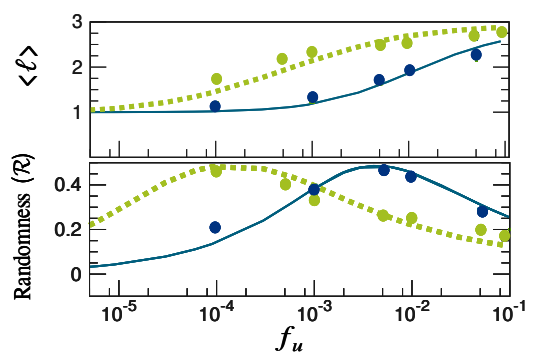


FIG. 4. Mean field predictions for (a) average length  $\langle \ell \rangle$  of rods, and (b) randomness parameter  $\mathcal{R}$  associated with rod length are plotted against fusion rate  $f_u$  for fixed values  $N = 3$  and  $f_i = 10^{-4}$ .  $\alpha = 0.9, \beta = 0.05$  correspond to  $\rho_c \simeq 0.9$  (dotted green) whereas  $\alpha = 0.05, \beta = 0.5$  correspond to  $\rho_c \simeq 0.1$  (continuous blue). (Lines-MFT ; Dots-Simulation).

heterogeneous dynamic population of all species of rods having lengths  $\ell = 1, 2, \dots, N$  is observed (see Fig.2).

#### Results under OBC -

By fixing  $\alpha = 0.15$  and  $\beta = 0.85$ , we have obtained the number-density profile and number flux profile plotted in Fig.3. In the fusion dominated regime, as the rods of length  $\ell = 1$  enter through  $i = 1$  and move forward, the population of longer rods increase at the expense of that of smaller rods because of the dominance of fusion. The populations of all the  $N$  species continue to evolve over a TZ at the end of which, marked by a vertical line in Fig.3, they attain their respective stationary values. For a given set of entry and exit rates, relative strength of fusion and fission determines the width of the TZ. The higher is the fusion rate, the narrower is the TZ (See Fig.3). Rods of length  $N$  dominate the population beyond the TZ if the coverage density is high enough for facilitating fusion.

Unlike the results obtained under PBC, which were dependent on  $f_u$  and  $f_i$  only through the ratio  $K = f_u/f_i$ , those under OBC depend on the individual rates  $f_u$  and

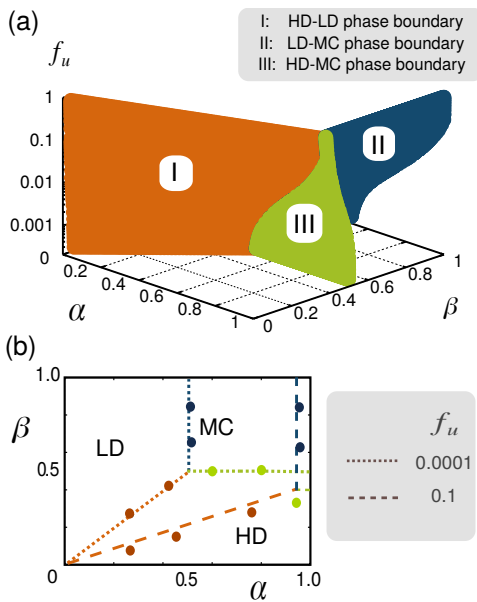


FIG. 5. Phase diagram of the model under OBC for  $N=3$  obtained using the extremum current hypothesis. (a) The 3D phase diagram is plotted in  $\alpha - \beta - f_u$  space. (b) 2D cross sections of the 3D phase diagram, for three values of  $f_u$ , are projected on the  $\alpha - \beta$  plane. (Lines-MFT ; Dots-Simulation)

$f_i$ . Moreover, unlike the attachment and detachment events of Langmuir kinetics [27], which depend solely on the occupation of a single sites, the fusion show a certain nonlinear dependence on the coverage density or occupation probability of a site. First, for a successful fusion event, both neighboring sites must be occupied simultaneously. And second, there is a bound on the maximum allowed length of the rods that can result from fusion.

Beyond the TZ, where the populations of the rods of different length remain stationary, we computed the average length of the rods  $\langle \ell \rangle$  as well as the randomness parameter  $\mathcal{R}$  (See Fig.4). By fixing the magnitude of  $f_i$ , we varied  $f_u$  over several orders of magnitudes. The average length of the rods varied from  $\langle \ell \rangle = 1.00$  in the fission dominated regime to  $\langle \ell \rangle = 3.00$  in the fusion dominated regime (maximum allowed length being  $N = 3$ ). But the randomness parameter  $\mathcal{R}$  exhibits a nonmonotonic variation with increasing  $f_u$ . Since fusion of two rods is allowed only if they touch each other, a higher coverage density  $\rho_c$  is expected to facilitate more frequent fusion. This is consistent with Fig.4(a) where, for a given  $f_u$ ,  $\langle \ell \rangle$  is higher at higher  $\rho_c$ . Moreover, in Fig.4(b) the curve essentially shifts laterally rightward because for attaining the same value of  $\mathcal{R}$  at lower coverage density a higher rate of fusion is required.

*Phase Diagram* The analytical results obtained under PBC are exploited in plotting the phase diagram under OBC using the *extremum current hypothesis* (ECH) [28–33]. For the implementation of ECH, first, one needs the expression for  $\rho_c^*$  (Fig.2). Next, one imagines a scenario

where the entry and exit points of the actual physical system are assumed to be coupled to two mass reservoirs of densities  $\rho_-$  and  $\rho_+$  respectively (see Fig.1), and calculates  $\rho_{\pm}$  using the expressions for flux derived under PBC. Equating both the incoming and outgoing flux at entry site 1, we solve for  $\rho_-$  as a function of entry rate  $\alpha$ ,  $f_u$  and  $f_i$ . Similarly, equating the incoming and outgoing flux at exit site  $L$  gives  $\rho_+$  as function of exit rate  $\beta$ ,  $f_u$  and  $f_i$  (see SI for the detailed derivation).

Fixing  $f_i=0.01$ , and taking constant cross sections of this 3D phase diagrams for three different values of  $f_u$  we plot the projections of these three cross sections onto the  $\alpha - \beta$  plane, as shown in Fig.5. In the limit  $f_u \ll f_i$  the phase boundaries approach those for single-species TASEP with  $\ell = 1$ . In the opposite limit  $f_u > f_i$ , all the HD-MC boundary shifts downwards as system tends to, effectively, a single species TASEP with rod-length  $\ell = N$  ( $N = 3$  in this case). But LD-MC phase boundary shifts towards right because, in order to form more rods of  $\ell = 3$  in the fusion dominated regime, rods of  $\ell = 1$  must enter at a higher rate  $\alpha$  so that interparticle distance between them shorten to facilitate effective fusion.

*Summary and Biological implications:* Motivated by the fusion and fission of cargoes in intraflagellar transport, in this letter we have developed a multi-species exclusion model where rods enter the lattice as single particles (i.e., as rods of length  $\ell = 1$ ), but their length change dynamically because of fusion and fission as the rods hop forward. We have demonstrated how the kinetics control the width of a ‘transition zone’ adjacent to the point of entry into the system. The term ‘transition zone’ in our theory should not be confused with the usage of the term in biology to describe a subcellular compartment that is believed to be present between the flagellar base and flagellum. We have also presented a mean-field theory for the distribution of the lengths of the rods as well as their density- and flux-profiles; the results are in excellent agreement with the numerical data obtained from Monte Carlo simulations (see SI for the detailed comparison).

Each eukaryotic flagellum consists of multiple (normally 9+2) doublets of antiparallel microtubules (MTs). Tipward (anterograde) transport of IFT trains occur along one MT while oppositely directed transport takes place in the other member of the doublet. The rates of the various kinetic processes in anterograde transport may be different from the corresponding ones in retrograde transport. This differences may result in different length distributions as well as density profiles and flux profiles in anterograde and retrograde transport. The transport on the two members of each doublet are likely to be coupled. Therefore, appropriate generalizations of our model is necessary before it can account for the numerical data on IFT collected from experiments on any specific organism. Nevertheless, conceptual and mathematical framework developed here may serve as foundation of the theoretical approach to be adopted for a complete description of IFT [37].

## ACKNOWLEDGEMENT

SP thanks Soumendu Ghosh and Bhavya Mishra for useful discussions. DC thanks Jonathon Howard for useful suggestions, Gunter Schütz for valuable comments on a preliminary version of this manuscript and Prabal K.

Maiti for hospitality at IISc, under the “DST MathBio” program, during the preparation of this manuscript. This work is supported by “Prof. S. Sampath Chair” Professorship (DC) and a J.C. Bose National Fellowship (DC).

## REFERENCES

- 
- [1] R. Blythe and M.R. Evans, *J. Phys. A* (2007).
- [2] M.R. Evans and T. Hanney, *J. Phys. A* **38**, R195 (2005).
- [3] P.L.Krapivsky, S. Redner and E. Ben-Naim, *A Kinetic view of Statistical Physics*, (Cambridge Univ. Press, 2010).
- [4] G.M. Schütz, in: *Phase Transitions and Critical Phenomena*, eds. C. Domb and J.L. Lebowitz (Academic Press, 2001).
- [5] B. Derrida, *Phys. Rep.* **301**, 65 (1998).
- [6] K. Mallick, *Physica A* **418**, 17 (2015).
- [7] R.K.P. Zia and B. Schmittmann, *J. Stat. Mech.:Theor and Expt.* P07012 (2007).
- [8] G. Schönherr and G.M. Schütz, *J. Phys. A* **37**, 8215 (2004).
- [9] J.J. Dong, B. Schmittmann and R.K.P. Zia, *Phys. Rev. E* **76**, 051113 (2007).
- [10] B. Mishra and D. Chowdhury, *Phys. Rev. E* **95**, 062117 (2017).
- [11] G.M. Schütz, *J. Phys. A* **36**, 051113 (2003).
- [12] A. Schadschneider, D. Chowdhury and K. Nishinari, *Stochastic transport in complex systems: from molecules to vehicles*, (Elsevier, 2010).
- [13] T. Chou, K. Mallick and R.K.P. Zia, *Rep. Prog. Phys.* **74**, 116601 (2011).
- [14] C. Appert-Rolland, M. Ebbinghaus and L. Santen, *Phys. Rep.* **593**, 1 (2015).
- [15] R. Lipowsky, Y. Chai, S. Klumpp, S. Liepelt and M.J. I. Müller, *Physica A* **372**, 34 (2006).
- [16] S. Muhuri and I. Pagonabarraga, *Phys. Rev. E* **82**, 021925 (2010).
- [17] P. Greulich, L. Ciandrini, R.J. Allen and M.C. Romano, *Phys. Rev. E* **85**, 011142 (2012).
- [18] A. Parmeggiani, I. Neri and N. Kern, in: *The Impact of Applications on Mathematics. Mathematics for Industry*, vol.1, eds. M. Wakayama et al. (Springer, 2014).
- [19] K.E.P. Sugden, M.R. Evans, W.C.K. Poon and N.D. Read, *Phys. Rev. E* **75**, 031909 (2007).
- [20] M.R.Evans, Y. Kafri, K.E.P. Sugden and J. Tailleur, *J. Stat. Mech. Theor. Expt.*, P06009 (2011).
- [21] L. Stepanek and G. Pigino, *Science* **352**, 721 (2016).
- [22] J. Buisson et al. *J. Cell Sci.* **126**, 327 (2012).
- [23] H. Ishikawa and W.F. Marshall, *CSH Perspectives in Biol* **9**, a021998 (2017).
- [24] K.F. Lehtreck KF et al. *Traffic.* **18**, 77 (2017).
- [25] J.J. Dong, S. Klumpp and R.K.P. Zia, *Phys. Rev. Lett.* **109**, 130602 (2012).
- [26] I.Pinkoviezky and N.S. Gov, *Phys. Rev. E* **89**, 052703 (2014).
- [27] A. Parmeggiani, T. Franosch and E. Frey, *Phys. Rev. Lett.* **90**, 086601 (2003).
- [28] J. Krug, *Phys. Rev. Lett.* **67**, 1882 (1991).
- [29] V. Popkov and G.M. Schütz, *Europhys. Lett.* **48**, 257 (1999).
- [30] T. Antal and G.M. Schütz, *Phys. Rev. E* **62**, 83 (2000).
- [31] V. Popkov and I. Peschel, *Phys. Rev. E* **64**, 026126 (2001).
- [32] J. Hager, *Phys. Rev. E* **63**, 067103 (2001).
- [33] J. Hager, J. Krug, V. Popkov and G.M. Schütz, *Phys. Rev. E* **63**, 056110 (2001).
- [34] D. Chowdhury, *Phys. Rep.* 529, 1 (2013).
- [35] A.B. Kolomeisky, *Motor proteins and molecular motors*, (CRC Press, 2015).
- [36] B. Engel, W. Ludington, and W. Marshall, *J. Cell Biol.* **187**, 81 (2009).
- [37] S. Patra and D. Chowdhury (in preparation, 2017)

**SUPPLEMENTARY INFORMATION**  
**A MULTISPECIES EXCLUSION PROCESS WITH FUSION AND FISSION OF RODS:**  
**A MODEL INSPIRED BY INTRAFLAGELLAR TRANSPORT**

**Swayamshree Patra and Debashish Chowdhury**

Department of Physics, Indian Institute of Technology Kanpur, 208016, India

**I. ALGORITHM FOR MC SIMULATION OF THE MODEL FOR ARBITRARY N**

Here we sketch the algorithm that we adopted for MC simulation of our model. The lattice sites, which are denoted by the integers  $i$  ( $1 \leq i \leq L$ ), are chosen randomly with equal probability using a good random number generator. The status of the site is then updated according to the kinetics that defines the model. A total of  $L$  successive updates constitutes a single MC step which is interpreted to corresponds to a real time interval  $\Delta t$ . If the randomly chosen site  $i$  happens to accommodate the leftmost tip of a rod, then the rod hops forward, with a hopping probability  $p dt$ , provided the downstream site ( $i+\ell$ ) is empty. Both its front and back end can also fuse with an equal probability  $f_u dt$  if and only if there is another rod of length ( $\ell'$ ) covering the neighbouring site and provided  $\ell' + \ell \leq N$ . Otherwise the attempt for fusion fails. In addition, the chosen rod of length  $\ell$  can split with probability  $f_i dt$  where all possible pairs  $\{\ell', \ell''\}$  that satisfy  $\ell' + \ell'' = \ell$  are equally probable result of a fission event. Note that, in the bulk, the rates are chosen in such a manner that the corresponding probabilities are normalized, i.e.,  $(2f_u + f_i + p)dt \leq 1$ . Similarly, total probabilities are also normalized at the two boundaries of the lattice.

**II. MASTER EQUATIONS UNDER PBC FOR ARBITRARY N**

In the main text we presented our analysis exclusively for the special case  $N=3$ . Here we present the master equations for an arbitrary value of the integer  $N$ . As described in the main text, the probability of finding a rod of length  $\ell$  at site  $i$  at time  $t$  is denoted by  $P_\ell(i, t)$ . Time evolution of  $P_\ell(i, t)$  ( $1 \leq \ell \leq N$ ) are given by the following master equations

$$\begin{aligned}
 \frac{dP_\ell(i, t)}{dt} = & \overbrace{pP_\ell(i-1, t)\xi_N(i-1|i+\ell-1) - pP_\ell(i, t)\xi_N(i|i+\ell)}^{\text{HOPPING terms}} \\
 & + \overbrace{f_i \sum_{s=\ell+1}^N \left(\frac{1}{s-1}\right) P_s(i, t)}^{\text{gain by FISSION}} + \overbrace{f_i \sum_{s=\ell+1}^N \left(\frac{1}{s-1}\right) P_s(i-s+\ell, t)}^{\text{gain by FISSION}} \\
 & \quad \text{fission of a rod of length } s(>\ell) \text{ located at } i \quad \text{fission of a rod of length } s(>\ell) \text{ located at } i-s \\
 & + \overbrace{f_u \sum_{s=1}^{\ell-1} P_s(i)P_{\ell-s}(i+s)}^{\text{gain by FUSION}} - \overbrace{f_i P_\ell(i, t)}^{\text{loss by FISSION}} \\
 & \quad \text{fusion of a rod of length } s \text{ at } i \text{ with a rod of length } \ell-s \text{ at } i+s \quad \text{fission of a rod of length } \ell \text{ located at } i \\
 & - \overbrace{f_u \sum_{s=1}^{N-\ell} P_\ell(i, t)P_s(i+\ell, t)}^{\text{loss by FUSION}} - \overbrace{f_u \sum_{s=1}^{N-\ell} P_\ell(i, t)P_s(i-s, t)}^{\text{loss by FUSION}} \\
 & \quad \text{fusion of rod of length } \ell \text{ at } i \text{ with rod of length } s \text{ at } i+\ell \quad \text{fusion of rod of length } \ell \text{ at } i \text{ with rod of length } s \text{ at } i-s
 \end{aligned} \tag{4}$$

for all  $i$  ( $1 \leq i \leq L$ ).

### III. DERIVATION OF CONDITIONAL PROBABILITY

The mutual exclusion in our model is captured by  $\xi_{N,\ell}(\underline{i}|i+\ell)$  which denotes the conditional probability that the site  $i+\ell$  is not occupied by another rod, given that there is a rod of length  $\ell$  at site  $i$ . In the steady state under periodic boundary condition, each site is treated under same footing. In this case, translation invariance follows naturally and  $\xi_{N,\ell}(\underline{i}|i+\ell) = \xi_{N,\ell}(\underline{1}|1+\ell)$ . So here we present the main steps of our calculation of  $\xi_{N,\ell}(\underline{1}|1+\ell)$ .

We first consider the special case  $N=2$ . Let the symbol  $Z(L, N_1, N_2)$  represent the number of ways of arranging  $N_1$  rods of length 1,  $N_2$  rods of length 2 and  $L - N_1\ell_1 - N_2\ell_2$  gaps and it is given by

$$Z(L, N_1, N_2) = \frac{(N_1 + N_2 + L - N_1 - 2N_2)!}{(N_1 + N_2)!(L - N_1 - 2N_2)!} \quad (5)$$

Number of ways of fixing a rod of length  $\ell = 1$  at site  $i = 1$  is given by  $Z(L - 1, N_1 - 1, N_2)$ . Out of these, number of ways of fixing a rod of length  $\ell = 1$  at site  $i = 2$  is  $Z(L - 2, N_1 - 2, N_2)$  [ $Z(L - 1 - 2, N_1 - 1, N_2 - 1)$ ]. Therefore, given that there is a rod of length  $\ell = 1$  at site  $i$ , probability of finding a rod of length  $\ell = 1$  at site  $i = 2$  is

$$\mathcal{P}(\underline{1}|1+\ell) = \frac{Z(L - 2, N_1 - 2, N_2)}{Z(L - 1, N_1 - 1, N_2)} = \frac{(N_1 + N_2 - 1)}{(L + N_1 + N_2 - 1N_1 - 2N_2 - 1)} \quad (6)$$

which is also equal to probability of finding a rod of length  $\ell = 2$  at  $i = 2$  given a rod of length  $\ell = 1$  at  $i = 1$ . Therefore, we conclude that probability of finding  $i = 2$  unoccupied provided  $i = 1$  is occupied by a rod of length  $\ell = 1$  is

$$\xi_{2,1}(\underline{i}|i+1) = \frac{(L - N_1 - 2N_2)}{(L + N_1 + N_2 - N_1 - 2N_2 - 1)} \quad (7)$$

Calculation shows that

$$\xi_{2,1}(\underline{i}|i+1) = \xi_{2,2}(\underline{i}|i+2) \quad (8)$$

i.e, conditional probability that the site  $i+1$  is not occupied by another rod, given that there is a rod of length  $\ell = 1$  at site  $i$  is equal to the conditional probability that the site  $i+2$  is not occupied by another rod, given that there is a rod of length  $\ell = 2$  at site  $i$ .

So, for  $N=2$  using the compact notation  $\xi_2$  for  $\xi_{2,1} = \xi_{2,2}$ , which denotes if a rod of length  $\ell$  ( $\ell = 1/\ell = 2$ ) occupies site  $i$ , probability of finding site  $i+\ell$  unoccupied is given by

$$\xi_2(\underline{i}|i+\ell) = \frac{(L - N_1 - 2N_2)}{(L + N_1 + N_2 - N_1 - 2N_2 - 1)} \quad (9)$$

Introducing the number densities  $\rho_1(N_1/L)$  and  $\rho_2(N_2/L)$ , above can be reexpressed as

$$\xi_2(\underline{i}|i+\ell) = \frac{1 - \rho_1 - 2\rho_2}{1 + \rho_1 + \rho_2 - \rho_1 - 2\rho_2} \quad (10)$$

As identity of each rod is constantly changing according to  $f_u$  and  $f_i$  rates,  $\rho_1$  and  $\rho_2$  keep fluctuating. Therefore we replace it with number probabilities  $P_1$  and  $P_2$  and get

$$\xi_2(\underline{i}|i+\ell) = \frac{1 - \sum_{s=1}^1 P_1(i+s) - \sum_{s=1}^2 P_2(i+s)}{1 + P_1(i+1) + P_2(i+2) - \sum_{s=1}^1 P_1(i+s) - \sum_{s=1}^2 P_2(i+s)} \quad (11)$$

Beauty of the conditional probability (11) is that, when  $\rho_2 = 0$ , it reduces to the  $(1-\rho_1)$  which is the conditional probability to be used for exclusion processes with particles. And when  $\rho_1 = 0$  it reduces to  $\frac{1-2\rho_2}{1+\rho_2-2\rho_2}$  which is the conditional probability to be used for exclusion processes with hard rods of length  $\ell = 2$ .

Similarly, it can be showed that the conditional probability for  $N=3$  is given by

$$\xi_3(\underline{i}|i+\ell) = \frac{1 - \sum_{s=1}^1 P_1(i+s) - \sum_{s=1}^2 P_2(i+s) - \sum_{s=1}^3 P_3(i+s)}{1 + P_1(i+1) + P_2(i+2) + P_3(i+3) - \sum_{s=1}^1 P_1(i+s) - \sum_{s=1}^2 P_2(i+s) - \sum_{s=1}^3 P_3(i+s)} \quad (12)$$

Hence, the generalised conditional probability for arbitrary  $N$  is given by

$$\xi_N(\underline{i}|i+\ell) = \frac{1 - \sum_{j=1}^N \{ \sum_{k=1}^j P_j(i+k) \}}{1 + \sum_{j=1}^N P_j(i+j) - \sum_{j=1}^N \{ \sum_{k=1}^j P_j(i+k) \}} \quad (13)$$

#### IV. RESULTS UNDER PBC

In this section, using the mean-field equations which govern the evolution of multispecies TASEP (4) and the conditional probabilities (13), we will analyse the results of for the special cases of N=2 and N=3 under periodic boundary conditions(PBC).

Master-equations governing the evolution of rods for N=2 are

$$\begin{aligned} \frac{dP_1(i,t)}{dt} = & \underbrace{pP_1(i-1)\xi_2 - pP_1(i)\xi_2}_{\text{hopping terms}} + \underbrace{f_i P_2(i,t) + f_i P_2(i-1,t)}_{\text{gain by fission of } \ell = 2} \\ & - \underbrace{f_u P_1(i)P_1(i+1)}_{\text{loss by fusing with a rod stalled ahead}} - \underbrace{f_u P_1(i)P_1(i-1)}_{\text{loss by fusing with a rod stalled behind}} \end{aligned} \quad (14)$$

$$\frac{dP_2(i,t)}{dt} = \underbrace{pP_2(i-1)\xi_2 - pP_2(i)\xi_2}_{\text{hopping terms}} + \underbrace{f_u P_1(i)P_1(i+1)}_{\text{gain by fusion of } \ell = 1} - \underbrace{f_i P_2(i,t)}_{\text{loss by fission}} \quad (15)$$

Master-equation governing the evolution of rods for N=3 are

$$\begin{aligned} \frac{dP_1(i)}{dt} = & \underbrace{pP_1(i-1)\xi_3 - pP_1(i)\xi_3}_{\text{hopping terms}} + \underbrace{f_i P_2(i) + f_i P_2(i-1) + \frac{f_i}{2} P_3(i) + \frac{f_i}{2} P_3(i-2)}_{\text{gain by fission of } \ell = 2 \text{ and } \ell = 3} \\ & - \underbrace{f_u P_1(i)P_1(i+1) - f_u P_1(i)P_1(i-1)}_{\text{loss by fusing with a rod stalled in the neighborhood}} \\ & - \underbrace{f_u P_1(i)P_2(i+1) - f_u P_1(i)P_2(i-1)}_{\text{loss by fusing with a rod stalled in the neighborhood}} \end{aligned} \quad (16)$$

$$\begin{aligned} \frac{dP_2(i)}{dt} = & \underbrace{pP_2(i-1)\xi_3 - pP_2(i)\xi_3}_{\text{hopping terms}} + \underbrace{\frac{f_i}{2} P_3(i) + \frac{f_i}{2} P_3(i-1)}_{\text{gain by fission of } \ell = 3} + \underbrace{f_u P_1(i)P_1(i+1)}_{\text{gain by fusion}} \\ & - \underbrace{f_u P_2(i)P_1(i+2) - f_u P_2(i)P_1(i-1)}_{\text{loss by fusion}} - \underbrace{f_i P_2(i)}_{\text{loss by fission}} \end{aligned} \quad (17)$$

$$\frac{dP_3(i)}{dt} = \underbrace{pP_3(i-1)\xi_3 - pP_3(i)\xi_3}_{\text{hopping terms}} - \underbrace{f_i P_3(i)}_{\text{loss by fission}} + \underbrace{f_u P_1(i)P_2(i+1) + f_u P_2(i)P_1(i+2)}_{\text{gain by fusion}} \quad (18)$$

We define  $K = f_u/f_i$  as the stickiness parameter.

Due to translation symmetry under PBC, equations for N=2 reduce to

$$K P_1^2 - P_2 = 0 \quad (19)$$

subjected to the constraint

$$P_1 + 2P_2 = \rho_c \quad (20)$$

and for N=3 will reduce to

$$\begin{aligned} 2K P_1 P_2 - P_3 &= 0 \\ K P_1^2 - P_2^2 &= 0 \end{aligned} \quad (21)$$

subjected to the constraint

$$P_1 + 2P_2 + 3P_3 = \rho_c \quad (22)$$

Hence, we conclude, under PBC, system of  $N$  equations describing the multispecies TASEP, will reduce to  $N - 1$  equations subjected to the following mass conservation constraint

$$\sum_{\ell=1}^N \ell P_\ell = \rho_c \quad (23)$$

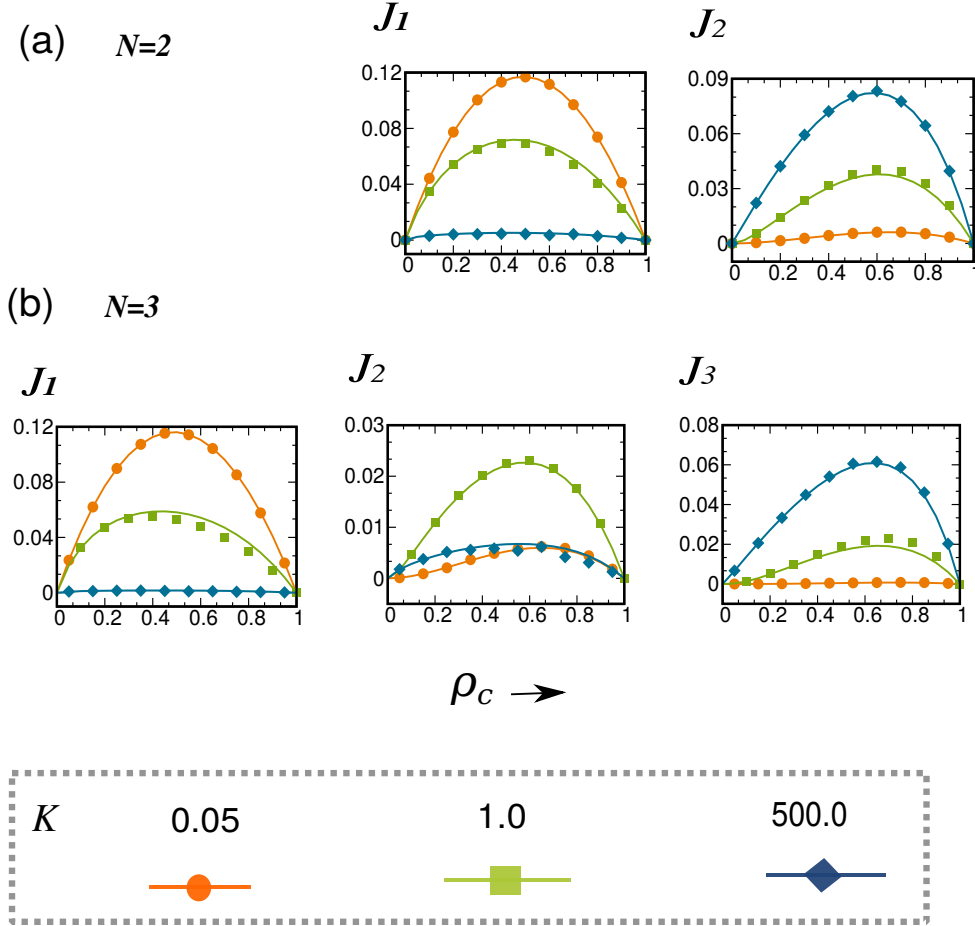


FIG. 6. Species specific Flux Profiles under PBC for different values of stickiness  $K$  for (a)  $N=2$  (b)  $N=3$  and (c)  $N=3$  cases (Lines–MFT ; Dots–Simulation)

In Table II, all the  $\ell$ -dependent quantities and in Table III all collective quantities are summarised for  $N=2,3$ . Number densities and other quantities are expressed in compact form using the terms  $\zeta_{N,n}$  ( $n=1,2,\dots,N-1$ ) which are the functions of  $\rho_c$  and  $K$ . These are

$$\zeta_{2,1} = \frac{\sqrt{1 + 8K\rho_c} - 1}{4K} \quad (24)$$

$$\zeta_{3,1} = -\frac{1}{9K} - \frac{7}{9 \cdot 2^{1/3} \left( 23K^3 + 243K^4\rho_c + 9\sqrt{3}\sqrt{5K^6 + 46K^7\rho_c + 243K^8\rho_c^2} \right)^{1/3}} + \frac{\left( 23K^3 + 243K^4\rho_c + 9\sqrt{3}\sqrt{5K^6 + 46K^7\rho_c + 243K^8\rho_c^2} \right)^{1/3}}{9 \cdot 2^{2/3} K^2} \quad (25)$$

TABLE II.  $\ell$ -dependent Quantities For N=2 and N=3

N	$\ell = 1$	$\ell = 2$	$\ell = 3$
<b>Number Density (<math>\mathcal{P}_\ell</math>)</b>			
N=2	$\zeta_{2,1}$	$\frac{1}{2}(\rho_c - \zeta_{2,1})$	
N=3	$\zeta_{3,1}$	$\zeta_{3,2} - \frac{2}{9}\zeta_{3,1}$	$\frac{\rho_c}{3} - \frac{5}{27}\zeta_{3,1} - \frac{2}{3}\zeta_{3,2}$
<b>Number Flux (<math>\mathcal{J}_\ell</math>)</b>			
N=2	$\frac{2p(1-\rho_c)\zeta_{2,1}}{(2-\rho_c)+\zeta_{2,1}}$	$\frac{p(1-\rho_c)(\rho_c-\zeta_{2,1})}{(2-\rho_c)+\zeta_{2,1}}$	
N=3	$\frac{27p(1-\rho_c)\zeta_{3,1}}{16\zeta_{3,1}+9(3+2\zeta_{3,2}-2\rho_c)}$	$\frac{3p(1-\rho_c)(9\zeta_{3,2}-2\zeta_{3,1})}{16\zeta_{3,1}+9(3+2\zeta_{3,2}-2\rho_c)}$	$\frac{p(1-\rho_c)(9\rho_c-5\zeta_{3,1}-18\zeta_{3,2})}{16\zeta_{3,1}+9(3+2\zeta_{3,2}-2\rho_c)}$
<b>Fraction (<math>\mathcal{F}_\ell</math>)</b>			
N=2	$\frac{2\zeta_{2,1}}{\rho_c+\zeta_{2,1}}$	$\frac{\rho_c-\zeta_{2,1}}{\rho_c+\zeta_{2,1}}$	
N=3	$\frac{27\zeta_{3,1}}{9\rho_c+16\zeta_{3,1}+9\zeta_{3,2}}$	$\frac{27\zeta_{3,2}-6\zeta_{3,1}}{9\rho_c+16\zeta_{3,1}+9\zeta_{3,2}}$	$\frac{9\rho_c-5\zeta_{3,1}-18\zeta_{3,2}}{9\rho_c+16\zeta_{3,1}+9\zeta_{3,2}}$

$$\zeta_{3,2} = -\frac{8}{81K} + \frac{49K}{81 \cdot 2^{2/3} \left( 23K^3 + 243K^4\rho_c + 9\sqrt{3}\sqrt{5K^6 + 46K^7\rho_c + 243K^8\rho_c^2} \right)^{2/3}} + \frac{\left( 23K^3 + 243K^4\rho_c + 9\sqrt{3}\sqrt{5K^6 + 46K^7\rho_c + 243K^8\rho_c^2} \right)^{2/3}}{162 \cdot 2^{1/3}K^3} \quad (26)$$

## V. MASTER EQUATIONS UNDER OBC

### A. For N=2

The mean field equations in OBC are as follows:

For  $i = 1$  :

$$\frac{P_1(i,t)}{dt} = \alpha(1 - P_1(i) - P_2(i)) - pP_1(i)\xi - fuP_1(i)P_1(i+1) + f_iP_2(i) \quad (27)$$

$$\frac{P_2(i,t)}{dt} = fuP_1(i)P_1(i+1) - pP_2(i)\xi - f_iP_2(i) \quad (28)$$

For  $i = 2$  to  $i = L - 2$  :

TABLE III. Other Quantities For N=2 and N=3

Quantity	N=2	N=3
$\mathcal{J}_{mass}$	$\frac{2p\rho_c(1-\rho_c)}{(2-\rho_c)+\zeta_{2,1}}$	$\frac{27p\rho_c(1-\rho_c)}{16\zeta_{3,1}+9(3+2\zeta_{3,2}-2\rho_c)}$
$\langle \ell \rangle$	$\frac{2\rho_c}{\rho_c+\zeta_{2,1}}$	$\frac{27\rho_c}{(9\rho_c+16\zeta_{3,1}+9\zeta_{3,2})}$
$\sigma_\ell$ (standard deviation)	$\sqrt{2}\sqrt{-\frac{\zeta_{2,1}(\zeta_{2,1}-\rho)}{(\zeta_{2,1}+\rho)^2}}$	$\sqrt{3}\sqrt{\frac{-224\zeta_{3,1}^2+81\zeta_{3,2}(-2\zeta_{3,2}+\rho_c)+\zeta_{3,1}(-414\zeta_{3,2}+306\rho_c)}{(16\zeta_{3,1}+9(\zeta_{3,2}+\rho_c))^2}}$
$\mathcal{R}$	$\frac{\sqrt{\frac{\zeta_{2,1}(-\zeta_{2,1}+\rho_c)}{(\zeta_{2,1}+\rho_c)^2}}(\zeta_{2,1}+\rho_c)}{\sqrt{2}\rho_c}$	$\frac{(16\zeta_{3,1}+9(\zeta_{3,2}+\rho_c))\sqrt{\frac{-224\zeta_{3,1}^2+81\zeta_{3,2}(-2\zeta_{3,2}+\rho_c)+\zeta_{3,1}(-414\zeta_{3,2}+306\rho_c)}{(16\zeta_{3,1}+9(\zeta_{3,2}+\rho_c))^2}}}{9\sqrt{3}\rho_c}$

$$\begin{aligned} \frac{P_1(i,t)}{dt} &= pP_1(i-1)\xi - pP_1(i)\xi - (fuP_1(i)P_2(i+1)) \\ &\quad - (fuP_1(i)P_1(i-1)) + fiP_2(i) + fiP_2(i-1) \end{aligned} \quad (29)$$

$$\frac{P_2(i)}{dt} = pP_2(i-1)\xi - pP_2(i)\xi + (fuP_1(i)P_1(i+1)) - fiP_2(i) \quad (30)$$

for  $i = L - 1$

$$\begin{aligned} \frac{P_1(i,t)}{dt} &= pP_1(i-1)\xi - pP_1(i+1)(1 - P_1(i+1) - P_2(i+1)) - fuP_1(i)P_1(i+1) \\ &\quad - fuP_1(i)P_1(i-1) + fiP_2(i) + fiP_2(i-1) \end{aligned} \quad (31)$$

$$\frac{dP_2(i)}{dt} = pP_2(i-1)\xi - pP_2(i) + fuP_1(i)P_1(i-1) - fiP_2(i) \quad (32)$$

for  $i = L$

$$\frac{dP_1(i)}{dt} = pP_1(i-1)(1 - P_1(i) - P_2(i)) - \beta P_1(i) - fuP_1(i)P_1(i-1) + fiP_2(i-1) \quad (33)$$

$$\frac{dP_2(i)}{dt} = pP_2(i-1) - \beta P_2(i) \quad (34)$$

### B. For N=3

For  $i = 1$

$$\frac{dP_1(i)}{dt} = \alpha(1 - P_1(i) - P_2(i) - P_3(i)) - pP_1(i)\xi - fuP_1(i)P_2(i+1) + fiP_2(i)$$

$$\frac{dP_2(i)}{dt} = -pP_2(i)\xi - fiP_2(i) + fuP_1(i)P_1(i+1) + \frac{f_i}{2}P_3(i) - fuP_2(i)P_1(i+2)$$

$$\frac{dP_3(i)}{dt} = -pP_3(i)\xi + fuP_2(i)P_1(i+2) + fuP_1(i)P_2(i+1) - fiP_3(i) \quad (35)$$

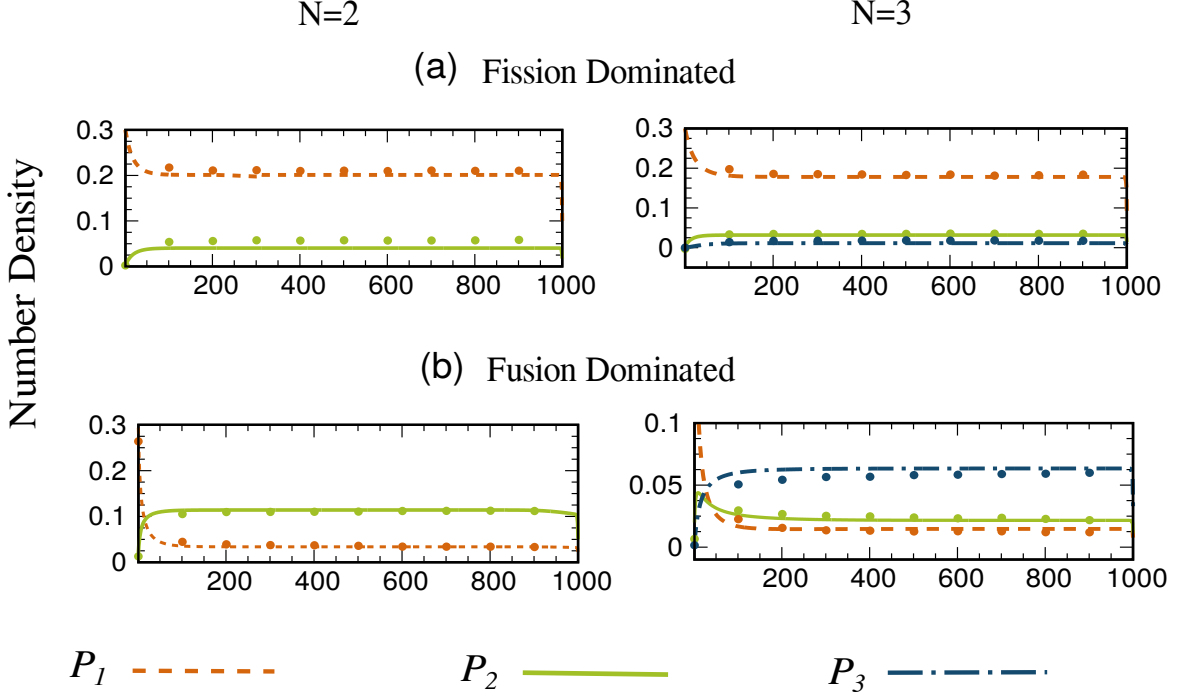


FIG. 7. Density Profiles for N=2 and N=3 cases :(a) fission dominated ( $f_u = 0.001$   $f_i = 0.01$ ) (b) fusion dominated ( $f_u = 0.01$   $f_i = 0.001$ ) regimes.  $\alpha = 0.15$  and  $\beta = 0.85$ . (Lines–MFT ; Dots–Simulation)

for  $i = 2$

$$\begin{aligned} \frac{dP_1(i)}{dt} &= pP_1(i-1)\xi - pP_1(i)\xi - f_u P_1(i)P_1(i+1) - f_u P_1(i)P_1(i-1) \\ &\quad - f_u P_1(i)P_2(i+1) + f_i P_2(i) + f_i P_2(i-1) + \frac{f_i}{2} P_3(i) \end{aligned}$$

$$\begin{aligned} \frac{dP_2(i)}{dt} &= (pP_2(i-1)\xi - pP_2(i)\xi) + f_u P_1(i)P_1(i+1) + \frac{f_i}{2}(P_3(i) + P_3(i-1)) - \frac{f_i}{2} P_2(i) \\ &\quad - f_u P_2(i)P_1(i+2) - f_u P_2(i)P_1(i-1) \end{aligned}$$

$$\begin{aligned} \frac{dP_3(i)}{dt} &= (pP_3(i-1)\xi - pP_3(i)\xi) + f_u P_2(i)P_1(i+2) + f_u P_1(i)P_2(i+1) \\ &\quad - f_i P_3(i) \end{aligned} \tag{36}$$

for  $i = 3 - 997$

$$\begin{aligned} \frac{dP_1(i)}{dt} &= pP_1(i-1)\xi - pP_1(i)\xi - f_u P_1(i)P_1(i+1) - f_u P_1(i)P_1(i-1) \\ &\quad - f_u P_1(i)P_2(i+1) - f_u P_1(i)P_2(i-2) + f_i P_2(i) \\ &\quad + f_i P_2(i-1) + \frac{f_i}{3} P_3(i) + \frac{f_i}{2} P_3(i-2) \end{aligned}$$

$$\begin{aligned} \frac{dP_2(i)}{dt} &= (pP_2(i-1)\xi - pP_2(i)\xi) + f_u P_1(i)P_1(i+1) + \frac{f_i}{2}(P_3(i) + P_3(i-1)) - f_i P_2(i) \\ &\quad - f_u P_2(i)P_1(i+2) - f_u P_2(i)P_1(i-1) \end{aligned}$$

$$\begin{aligned} \frac{dP_3(i)}{dt} &= pP_3(i-1)\xi - pP_3(i)\xi + f_u P_2(i)P_1(i+2) + f_u P_1(i)P_2(i+1) \\ &\quad - f_i P_3(i) \end{aligned} \tag{37}$$

For  $i = 998$

$$\begin{aligned}
\frac{dP_1(i)}{dt} &= pP_1(i-1)\xi - pP_1(i)(1 - P_1(i+1) - P_2(i+1) - P_3(i+1)) - f_u P_1(i)P_1(i+1) \\
&\quad - f_u P_1(i)P_1(i-1) - f_u P_1(i)P_2(i+1) - f_u P_1(i)P_2(i-2) \\
&\quad + f_i P_2(i) + f_i P_2(i-1) + \frac{f_i}{2} P_3(i) + \frac{f_i}{2} P_3(i-2) \\
\frac{dP_2(i)}{dt} &= pP_2(i-1)\xi - pP_2(i)(1 - P_1(i+1) - P_2(i+1) - P_3(i+1)) + f_u P_1(i)P_1(i+1) \\
&\quad + \frac{f_i}{2}(P_3(i) + P_3(i-1)) - \frac{f_i}{2} P_2(i) - f_u P_2(i)P_1(i+2) - f_u P_2(i)P_1(i-1) \\
\frac{dP_3(i)}{dt} &= pP_3(i-1)\xi - pP_3(i) + f_u P_2(i)P_1(i+2) + f_u P_1(i)P_2(i+1) \\
&\quad - f_i P_3(i)
\end{aligned} \tag{38}$$

For  $i = 999$

$$\begin{aligned}
\frac{dP_1(i)}{dt} &= pP_1(i-1)(1 - P_1(i) - P_2(i) - P_3(i)) - pP_1(i)(1 - P_1(i+1) - P_2(i+1) - P_3(i+1)) - f_u P_1(i)P_1(i+1) \\
&\quad - f_u P_1(i)P_1(i-1) - f_u P_1(i)P_2(i+1) \\
&\quad - f_u P_1(i)P_2(i-2) + f_i P_2(i) + f_i P_2(i-1) + \frac{f_i}{2} P_3(i) + \frac{f_i}{2} P_3(i-2) \\
\frac{dP_2(i)}{dt} &= pP_2(i-1)(1 - P_1(i) - P_2(i) - P_3(i)) - pP_2(i)(1 - P_1(i+1) - P_2(i+1) - P_3(i+1)) + f_u P_1(i)P_1(i+1) \\
&\quad + \frac{f_i}{2}(P_3(i) + P_3(i-1)) - f_i P_2(i) - f_u P_2(i)P_1(i-1) \\
\frac{dP_3(i)}{dt} &= pP_3(i-1) - pP_3(i) + f_u P_1(i)P_2(i+1) - f_i P_3(i)
\end{aligned} \tag{39}$$

For  $i = 1000$

$$\begin{aligned}
\frac{dP_1(i)}{dt} &= pP_1(i-1)(1 - P_1(i) - P_2(i) - P_3(i)) - \beta P_1(i) - f_u P_1(i)(P_1(i-1) + P_2(i-2)) \\
&\quad + f_i P_2(i-1) + \frac{f_i}{2} P_3(i-2) \\
\frac{dP_2(i)}{dt} &= pP_2(i-1) - \beta P_2(i) - f_u P_2(i)P_1(i-1) + \frac{f_i}{2} P_3(i-1) \\
\frac{dP_3(i)}{dt} &= pP_3(i-1) - \beta P_3(i)
\end{aligned} \tag{40}$$

## VI. PHASE DIAGRAM FOR MULTISPECIES TASEP

### A. Steps for Plotting the Phase Diagram

#### 1. Expressions for $\rho_+$ and $\rho_-$

At the entry site  $i = 1$ , the mass flux  $J_{in}^1$  moving into this site from the reservoir of density  $\rho_-$  is

$$J_{in}^1 = \alpha(1 - \rho_-). \tag{41}$$

The conditional probability of finding an empty site, provided that  $\ell$  sites on its left are covered by a rod of length  $\ell$  is  $P_\ell(\overbrace{\mathbf{1} \dots \mathbf{1}}^\ell | 0)$ . Therefore, the mass flux  $J_{out}^1$  moving out of the same site  $i = 1$  is given by

$$J_{out}^1 = \rho_- P_\ell(\overbrace{\mathbf{1} \dots \mathbf{1}}^\ell | 0) \tag{42}$$

where

$$P_\ell(\overbrace{\mathbf{1} \dots \mathbf{1}}^\ell | 0) = \frac{1 - \sum_{j=1}^N \{\sum_{k=1}^j P_j(i+k)\}}{1 + \sum_{j=1}^N P_j(i+j) - \sum_{j=1}^N \{\sum_{k=1}^j P_j(i+k)\}} \tag{43}$$

Substituting (43) into (42) and then equating the outgoing flux (42) with in incoming flux (41) at site 1 ( $J_{in}^1 = J_{out}^1$ ), we get an equation for  $\rho_-$  as a function of  $f_u$ ,  $f_i$  and  $\alpha$

$$\rho_- = \rho_-(\alpha, f_u, f_i) \quad (44)$$

Similarly,  $P_\ell(\underbrace{1\dots\dots 1}_\ell | 0)$  denotes the conditional probability that, given an uncovered site, there will be  $\ell$  adjacent sites to the left which are covered simultaneously by a rod of length  $\ell$ . So incoming flux at site  $i = L$  is

$$J_{in}^L = \rho_+ \mathcal{P}_\ell(\underbrace{1\dots\dots 1}_\ell | 0) \quad (45)$$

where

$$\mathcal{P}_\ell(\underbrace{1\dots\dots 1}_\ell | 0) = \frac{\sum_{j=1}^N P_j(i+j)}{1 + \sum_{j=1}^N P_j(i+j) - \sum_{j=1}^N \{\sum_{k=1}^j P_j(i+k)\}} \quad (46)$$

and the outgoing flux  $J_{out}^L$  is given by

$$J_{out}^L = \beta \rho_+. \quad (47)$$

Hence equating the incoming and outgoing fluxes (45) and (47), respectively, at  $i = L$  and solving the resulting equation for  $\rho_+$ , we get  $\rho_+$  as a function of  $f_u, f_i$  and  $\beta$

$$\rho_+ = \rho_+(\beta, f_u, f_i) \quad (48)$$

## 2. Surface separating LD-MC phases

According to the ECH, at the boundary between the LD and MC phases

$$\rho_-(\alpha, f_u, f_i) = \rho_c^* \quad (49)$$

Substituting the expressions (44) and appropriate  $\rho_c^*(K)$  in (49) we get the equation

$$\alpha^* = \alpha^*(\rho^*, f_u, f_i) \quad (50)$$

for the surface separating the LD and MC phases.

## 3. Surface separating HD-MC phases

According to the ECH, at the boundary between the HD and MC phases

$$\rho_+(\beta, f_u, f_i) = \rho_c^* \quad (51)$$

Substituting the expressions (48) and  $\rho_c^*(K)$  in (51) we get the equation

$$\beta^* = \beta^*(\rho^*, f_u, f_i) \quad (52)$$

for the surface separating the HD and MC phases.

## 4. Surface separating LD-HD phases

The equation for this surface is obtained by exploiting the fact that exactly on this surface the LD and HD phases coexist simultaneously in the system supporting a single steady state flux that flows through the system. Therefore, the corresponding condition can be implemented mathematically by

$$J_{PBC}(\rho_-(\alpha, f_u, f_i)) = J_{PBC}(\rho_+(\beta, f_u, f_i)) \quad (53)$$

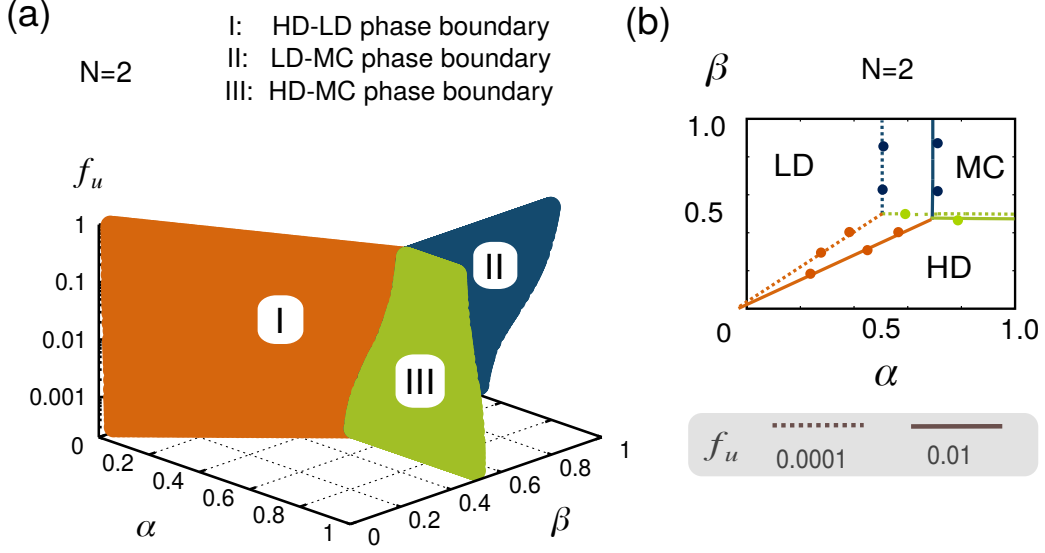


FIG. 8. Phase diagram of the model under OBC for  $N=2$ . (a) The 3D phase diagram is plotted in  $\alpha$   $\beta$   $f_u$  space. (b) 2D cross sections of the 3D phase diagram, for three different values of the parameter  $f_u$ , are projected on the  $\alpha\beta$  plane. Value of  $f_i$  is fixed at 0.01.

### B. Phase Boundaries for $N=2$

$$\alpha^* = -\frac{8f_u\rho^*}{f_i - 8f_u + 4f_u\rho^* - \sqrt{f_i}\sqrt{f_i + 8f_u\rho^*}} \quad (54)$$

$$\beta^* = \frac{f_i - 4f_u\rho^* - \sqrt{f_i}\sqrt{f_i + 8f_u\rho^*}}{f_i - 8f_u + 4f_u\rho^* - \sqrt{f_i}\sqrt{f_i + 8f_u\rho^*}} \quad (55)$$

$$\frac{-\alpha(f_i - 8f_u - 4f_u\alpha) + \alpha\sqrt{f_i}\sqrt{f_i + 8f_u\alpha} + 4f_u\alpha^2}{f_u(8 + 8\alpha + 2\alpha^2)} = \frac{f_i(1 - \beta) + 4f_u\beta + 4f_u\beta^2 + \sqrt{f_i}(-1 + \beta)\sqrt{f_i + 4f_u\beta + 4f_u\beta^2}}{f_u(2 + 4\beta + 2\beta^2)} \quad (56)$$

### C. Phase Boundaries for $N=3$

$$\alpha^* = \frac{A1}{A2 + A3 + A4 + A5} \quad (57)$$

$$\beta^* = \frac{B1 + B2 + B3 + B4}{B11 + B2 + B3 + B5} \quad (58)$$

where

$$A1 = 324f_i f_u^3 \rho_c \left( 23f_i^3 f_u^3 + 243f_i^2 f_u^4 \rho_c + 9\sqrt{3}\sqrt{f_i^4 f_u^6 (5f_i^2 + 46f_i f_u \rho_c + 243f_u^2 \rho_c^2)} \right)^{2/3} \quad (59)$$

$$A2 = 278 \cdot 2^{1/3} f_i^4 f_u^4 + 3 \cdot 2^{2/3} \sqrt{3} \sqrt{f_i^4 f_u^6 (5f_i^2 + 46f_i f_u \rho_c + 243f_u^2 \rho_c^2)} \left( 23f_i^3 f_u^3 + 243f_i^2 f_u^4 \rho_c + 9\sqrt{3}\sqrt{f_i^4 f_u^6 (5f_i^2 + 46f_i f_u \rho_c + 243f_u^2 \rho_c^2)} \right)^{1/3} \quad (60)$$

$$A3 = f_i^2 f_u^2 \left( 23f_i^3 f_u^3 + 243f_i^2 f_u^4 \rho_c + 9\sqrt{3}\sqrt{f_i^4 f_u^6 (5f_i^2 + 46f_i f_u \rho_c + 243f_u^2 \rho_c^2)} \right)^{1/3} \quad (61)$$

$$\left( 81 \cdot 2^{2/3} f_u^2 \rho_c - 32 \left( 23f_i^3 f_u^3 + 243f_i^2 f_u^4 \rho_c + 9\sqrt{3}\sqrt{f_i^4 f_u^6 (5f_i^2 + 46f_i f_u \rho_c + 243f_u^2 \rho_c^2)} \right)^{1/3} \right) \quad (62)$$

$$A4 = 12f_i \tag{63}$$

$$\left( 8 \cdot 2^{1/3} \sqrt{3} f_u \sqrt{f_i^4 f_u^6 (5f_i^2 + 46f_i f_u \rho_c + 243f_u^2 \rho_c^2)} - 9f_u^3 (-3 + 2\rho_c) \left( 23f_i^3 f_u^3 + 243f_i^2 f_u^4 \rho_c + 9\sqrt{3} \sqrt{f_i^4 f_u^6 (5f_i^2 + 46f_i f_u \rho_c + 243f_u^2 \rho_c^2)} \right)^{2/3} \right)$$

$$A5 = 2^{1/3} f_i^3 f_u^3 \left( 2592f_u^2 \rho_c - 67 \left( 46f_i^3 f_u^3 + 486f_i^2 f_u^4 \rho_c + 18\sqrt{3} \sqrt{f_i^4 f_u^6 (5f_i^2 + 46f_i f_u \rho_c + 243f_u^2 \rho_c^2)} \right)^{1/3} \right) \tag{64}$$

$$B1 = 278 \cdot 2^{1/3} f_i^4 f_u^4 + 3 \cdot 2^{2/3} \sqrt{3} \sqrt{f_i^4 f_u^6 (5f_i^2 + 46f_i f_u \rho_c + 243f_u^2 \rho_c^2)} \tag{65}$$

$$\left( 23f_i^3 f_u^3 + 243f_i^2 f_u^4 \rho_c + 9\sqrt{3} \sqrt{f_i^4 f_u^6 (5f_i^2 + 46f_i f_u \rho_c + 243f_u^2 \rho_c^2)} \right)^{1/3} \tag{66}$$

$$B2 = f_i^2 f_u^2 \left( 23f_i^3 f_u^3 + 243f_i^2 f_u^4 \rho_c + 9\sqrt{3} \sqrt{f_i^4 f_u^6 (5f_i^2 + 46f_i f_u \rho_c + 243f_u^2 \rho_c^2)} \right)^{1/3} \tag{67}$$

$$\left( 81 \cdot 2^{2/3} f_u^2 \rho_c - 32 \left( 23f_i^3 f_u^3 + 243f_i^2 f_u^4 \rho_c + 9\sqrt{3} \sqrt{f_i^4 f_u^6 (5f_i^2 + 46f_i f_u \rho_c + 243f_u^2 \rho_c^2)} \right)^{1/3} \right)$$

$$B3 = 12f_i \tag{68}$$

$$\left( 8 \cdot 2^{1/3} \sqrt{3} f_u \sqrt{f_i^4 f_u^6 (5f_i^2 + 46f_i f_u \rho_c + 243f_u^2 \rho_c^2)} + 9f_u^3 \rho_c \left( 23f_i^3 f_u^3 + 243f_i^2 f_u^4 \rho_c + 9\sqrt{3} \sqrt{f_i^4 f_u^6 (5f_i^2 + 46f_i f_u \rho_c + 243f_u^2 \rho_c^2)} \right)^{2/3} \right)$$

$$B4 = 2^{1/3} f_i^3 f_u^3 \left( 2592f_u^2 \rho_c - 67 \left( 46f_i^3 f_u^3 + 486f_i^2 f_u^4 \rho_c + 18\sqrt{3} \sqrt{f_i^4 f_u^6 (5f_i^2 + 46f_i f_u \rho_c + 243f_u^2 \rho_c^2)} \right)^{1/3} \right) \tag{69}$$

$$B5 = 12f_i \tag{70}$$

$$\left( 8 \cdot 2^{1/3} \sqrt{3} f_u \sqrt{f_i^4 f_u^6 (5f_i^2 + 46f_i f_u \rho_c + 243f_u^2 \rho_c^2)} - 9f_u^3 (-3 + 2\rho_c) \left( 23f_i^3 f_u^3 + 243f_i^2 f_u^4 \rho_c + 9\sqrt{3} \sqrt{f_i^4 f_u^6 (5f_i^2 + 46f_i f_u \rho_c + 243f_u^2 \rho_c^2)} \right)^{2/3} \right)$$

#### D. Interpreting Phase Diagram

Let  $\alpha^*$  and  $\beta^*$  represent the surface separating  $LD - MC$  and  $HD - MC$  phases respectively.

For conventional  $\ell$ -TASEP, i.e, TASEP with hard-rods of length  $\ell$  only, the known results are tabulated in the following Table.IV

TABLE IV. **Results for conventional  $\ell$ -TASEP**

$\ell$	$\rho^*$	$\alpha^* = \beta^*$
$\ell$	$\frac{\sqrt{\ell}}{\sqrt{\ell+1}}$	$\frac{1}{\sqrt{\ell+1}}$
1	0.5	0.5
2	0.58	0.41
3	0.63	0.36

Now to interpret the phase boundaries of our model with  $N = 2$  in extreme limit, we re-express equations (50) and (52) in terms of  $\zeta_{2,1}$  and  $\rho_c^*$  in Table V and show the approximations in extreme limits of  $f_u$ .

This could be understood as : In  $f_u \rightarrow 0$  limit, the phase diagram matches exactly with the phase diagram of particles (rods of  $\ell = 1$ ) as the particles have no tendency to fuse. In the opposite limit  $f_u > f_i$ , all the HD-MC boundary shifts downwards as system tends to, effectively, a single species TASEP with rod-length =  $N$  ( $N = 3$  in this case). But LD-MC phase boundary shifts towards right because, in order to form more rods of  $\ell = N$  in the fusion dominated regime, rods of  $\ell = 1$  must enter at a higher rate  $\alpha$  so that interparticle distance between them shorten to facilitate effective fusion. When  $f_u \rightarrow \infty$  the value of  $\beta^*$  matches with that of  $\ell$ -TASEP ( $\ell = N$ ) but  $\alpha^* = N\beta^*$  in this limit because for the formation of a rod of  $\ell = N$ ,  $N$  particles of  $\ell = 1$  must enter. Hence, it altogether shifts the LD-MC phase boundary ( $\alpha^*$ ) with increasing  $f_u$  in such a way that  $\alpha^* > \beta^*$  and becomes  $\alpha^* \approx N\beta^*$  in  $f_u \rightarrow \infty$  limit. The results for our model for arbitrary  $N$  are summarised in Table VI.

Another inference from the phase-diagram is that as we increase  $f_u$ , it is very difficult to get the MC phase.

TABLE V. Phase Boundaries in Extreme limits of  $f_u$  for  $N=2$  case

Quantity	Expression	$f_u \rightarrow 0$	$f_u \rightarrow \infty$
$\zeta$	$\frac{\sqrt{1+8(f_u/f_i)\rho_c-1}}{4(f_u/f+i)}$	$\rho_c$	$\approx 0$
$\alpha^*$	$\frac{2\rho_c^*}{2-\rho_c^*+\zeta}$	$\rho_c^*=0.5$	$2(\frac{\rho_c^*}{2-\rho_c^*}) \approx 0.82$
$\beta^*$	$\frac{\rho_c^*+\zeta}{2-\rho_c^*+\zeta}$	$\rho_c^*=0.5$	$\frac{\rho_c^*}{2-\rho_c^*} \approx 0.41$

TABLE VI. Phase Boundaries for arbitrary  $N$  in  $f_u \rightarrow \infty$  limit

$N$	$\alpha^*$	$\beta^*$
1	0.5	0.5
2	0.82	0.41
3	1.08	0.36
$N$	$\frac{N}{\sqrt{N+1}}$	$\frac{1}{\sqrt{N+1}}$

## VII. SPACE-TIME DIAGRAM

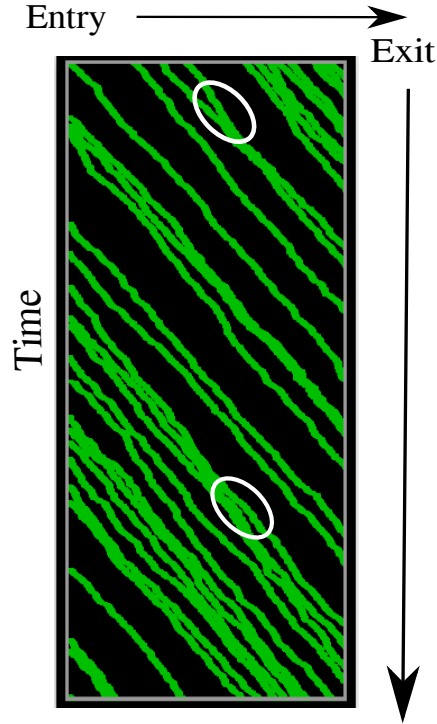


FIG. 9. Space-Time Diagram: Showing fusion and fission of rods